Role of interface on irradiation damage of Cu−diamond composites using classical molecular dynamics simulations

Yanan Jin [a], Hai Huang [a,b,*], Yinghui Zhong [a,b], Xiaoting Yuan [a], Huan Li [c], Ding Lou [a], Kun Xie [a], Zhongxia Liu [a], Bin Cai [a,b], Qing Peng [d]

[a] *Key Laboratory of Material Physics of Ministry of Education, School of Physics and Microelectronics, Zhengzhou University, Zhengzhou, 450052, China*
[b] *Institute of Intelligent Sensing, Zhengzhou University, Zhengzhou, 450001, China*
[c] *Xi'an Rare Metal Materials Institute Co. Ltd., Xi'an, 710016, China*
[d] *State Key Laboratory of Nonlinear Mechanics, Institute of Mechanics, Chinese Academy of Sciences, Beijing, 100190, China*

ARTICLE INFO

ABSTRACT

Cu−diamond composites have been proposed as a candidate thermal management material for spacecraft electronics. Nevertheless, irradiation effects on the composites remain poorly understood at present. Here we focus on investigating the influence of Cu−diamond interfaces (CDIs) on energetic displacement cascades using atomistic simulations. Results show that a primary knock-on atom of Cu (PKA-Cu) can induce more significant damage than a PKA-C. Under almost all circumstances, the statistically averaged fraction of surviving interstitials is not only lower than that of vacancies but also no more than 1. Because of the unique nature in the mobility and interactions with CDIs, Cu interstitials exhibit the lowest concentration among all defects in most cases. The high residual rate of displaced defects in diamond makes it relatively difficult to heal. The structural damage is mainly manifested in a short-range disorder of diamond and a long-range disorder of Cu after irradiation. At elevated temperatures, the atomic displacement region may form compact chain-like defects to restrain lattice loosening. Despite the above, CDIs could act as effective sinks to facilitate the recombination and/or annihilation of irradiation-induced defects in all scenarios. This study provides an important insight into the understanding of the microscopic evolution of irradiation defects for the composites.

1. Introduction

Future deep-space exploration requires electronic devices with versatility such as signal communication, detection, and attitude control [1,2]. To achieve a faster computing speed, spacecraft electronic devices become more integrated and keep shrinking minimum feature sizes, resulting in a significant improvement in power density [3–5]. Problems such as heat generation, thermal stress, and warpage will follow, affecting the regular operation of devices that is related to the long-term reliability of spacecraft [6–8]. Recently, it has put forward high requirements for efficient heat dissipation of spacecraft electronic devices [4,9,10]. Unfortunately, traditional thermal management materials like Mo–Cu, W–Cu alloys, BeO ceramics, and Al–SiC composites can hardly meet the requirements because of their low thermal conductivity, high coefficient of thermal expansion (CTE), or toxicity [11–13]. Benefiting from the advantages of Cu with highest cost performance as well as

diamond with the highest thermal conductivity in nature (up to 2,200 W/(m·K)), Cu−diamond composites (CDCs), owning to excellent thermal conductivity in theory and large-scale application potential, have been considered as one of the most promising thermal management materials [14–17]. Consequently, CDCs provide a feasible solution for the above stringent requirements.

Working in deep space, materials also must suffer harsh irradiation environments that include high-energy protons, electrons, α-particles, *etc.*, causing severe performance degradation [18,19]. Many studies have directly or indirectly observed the phenomenon in different materials [20–22]. In terms of CDCs, space irradiation may trigger changes in their thermal conductivity, CTE, and structural mechanics [13,23], which will seriously threaten the safe service of electronic devices and then shorten spacecraft's life. For example, Xie et al. [23] found that a decrement of 4.8% for thermal conductivity and an increment of 15.8% for bending strength occur in CDCs after ^{60}Co γ-ray irradiation with a

total dose of 2.3×10^5 rad. Nevertheless, to our best knowledge, there is still a lack of detailed understanding of the irradiation damage of CDCs since only very little literature has been reported. Especially, what role Cu−diamond interfaces (CDIs) play in the irradiation degradation of the composites is unclear.

Many irradiation studies on interface materials have shown that grain boundaries and phase boundaries, including metal−nanocarbon (or −nanocarbide) interfaces, can serve as sinks, effectively alleviating irradiation-induced defects [24–32]. For example, Huang et al. [28] reported that the existence of Ni–SiC nanoparticle interfaces can suppress the growth of He bubbles and thereby retard the He embrittlement and swelling of Ni-based alloys under 3 MeV He-ion irradiation with ion fluence up to 3×10^{20} ions·m^{-2} at 873 K. So et al. [29] indicated that Al−carbon nanotube interface still has a great help in reducing radiation hardening and embrittlement under He- or self-ion irradiation up to 72 displacements per atom. Yang et al. [31] performed *in situ* Kr-ion irradiation under transmission electron microscopy on Cu−graphene composites and found that the Cu−graphene interface even exhibits higher defect annihilation capability relative to the high-angle Cu grain boundary. Based on *ab initio* calculations, Yang et al. [32] demonstrated that the Cu−graphene interface provides a strong sink for trapping defects and gives rise to preferential sites for their recombination. So it can be inferred that the presence of CDIs should be able to slow down the irradiation degradation of the composites, prolonging the service life of the materials. However, further research for the irradiation effects of CDCs is still needed.

In recent decades, molecular dynamics (MD) simulations have been widely used to understand the creation, mobility, clustering, and interaction of irradiation-induced defects on the dimension of ps-nm [26,33–35]. The success of MD works in different materials suggests that it may be feasible to study the evolution of defects in displacement cascades in CDCs using MD within an affordable simulation time. Hence, in the present work, MD simulations were executed to investigate the irradiation damage near a CDI for elucidating the irradiation response of CDCs. Several concerns, including the evolution of irradiated defects, their stability, their interaction with the CDI, and the damaged configurations of CDCs, were discussed during cascade collisions related to the initial displacement conditions and ambient temperature. We showed that CDIs could act as effective sinks to facilitate the recombination and/or annihilation of irradiation-induced defects and thereby are expected to improve the irradiation tolerance of CDCs acting as thermal management materials for spacecraft electronics.

2. Simulation methodology

All simulations were carried out with parallel MD code LAMMPS [36], and the resulting samples were analyzed with visualization software OVITO [37]. The embedded atom method (EAM) potential [38], the Tersoff potential [39], and the Lennard-Jones potential [40] were adopted to describe the interactions between Cu atoms, the interactions among C atoms in diamond, and the Cu–C interactions, respectively. All the potentials were splined into short-range ZBL interactions [41]. For the simulations, a 144.6 Å × 144.6 Å × 144.6 Å cubic box was created. A diamond sphere with a radius of 30 Å, containing 19,981 C atoms, was inserted at the center of the box, while the remaining space was filled with 245,167 Cu atoms, as shown in Fig. 1 (a). Periodic boundary conditions were employed in all calculations. To release the stress, the CDI model was relaxed by conjugate gradient minimization, then equilibrated to nearly zero pressure at a certain temperature lasting for 10 ps. The atomic potential energy distribution of the ground state is exhibited in Fig. 1 (b), from which the interface region of about 10 Å thickness is very distinguishable according to the potential energy difference.

Initially, a primary knock-on atom (PKA), selected from any element (Cu or C) of the composites, was launched at a certain distance away from the interface. Note that the two different types of PKAs were defined as PKA-Cu and PKA-C, respectively. To avoid channeling, the PKA was incident along a high-index direction <135> passing through the center of the diamond. During displacement cascades, the outer layer with $2a_0$ (a_0, Cu lattice constant) thickness was forced to dissipate the heat using Nose-Hoover thermostat (NVT ensemble), while the evolution of other atoms was followed with a variable time step using NVE ensemble. The simulation was completed in 21 ps. Three different cases were considered to investigate the irradiation damage near a CDI. For the first case, the distance between PKA-Cu (or PKA-C) and the interface varied from 7 to 42 Å with an interval of 7 Å, when the PKA energy and simulation temperature was fixed to be 5 keV and 100 K, respectively. For the second case, the kinetic energy of PKA-Cu was set as 1, 3, 5, 7, or 10 keV, and the corresponding distance between PKA-Cu and the interface was specified as 14, 21, 21, 21, or 35 Å, respectively. The reasons for choosing these distances are consistent with those of previous studies [26,42]. The thermostat temperature was regulated to 100 K. For the last case, the simulation temperature was maintained at 100, 200, 300, 400, or 500 K, while the kinetic energy of PKA-Cu and the distance between PKA-Cu and the interface were determined to be 5 keV and 21 Å, respectively. All the simulation temperatures were taken from those of the space environments [43–45]. For statistical purposes, 15 independent MD runs for each case were carried out. The
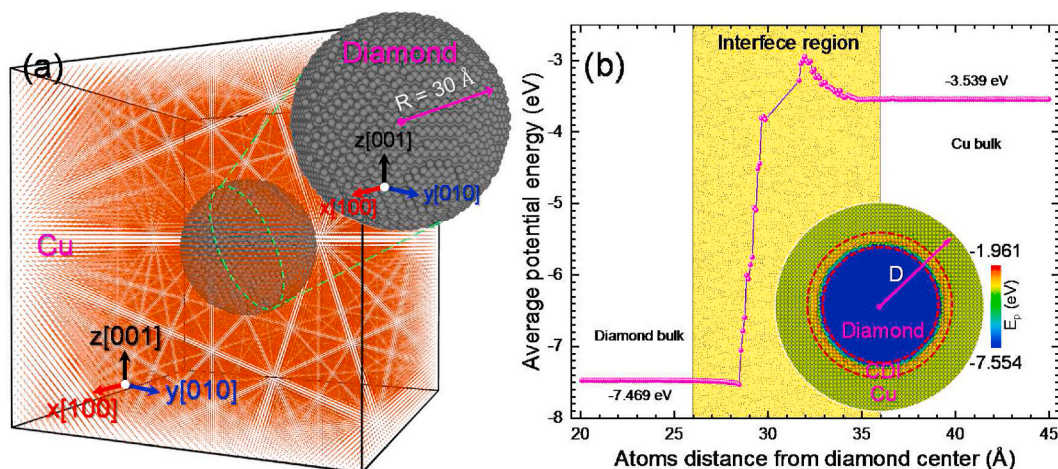

Fig. 1. Simulation model and its potential energy distribution of ground state. **(a)** Atomic configuration of CDCs. **(b)** Average potential energy of atoms in CDCs as a function of the radial distance with the diamond center as the origin. The interface region is highlighted.

irradiation-induced defects in the bulk were detected using Wigner–Seitz cell method [27,34]. In addition, the parameters for the cascade simulations of single-crystal Cu or diamond were the same as those of CDCs, facilitating the comparison.

3. Results and discussion

3.1. Defect evolution and distribution

To clarify the impact of CDIs on the defect formation stage or annealing stage, the typical evolution of defect number with time in the bulk is shown in Fig. 2, produced by a 5 keV PKA-Cu (or PKA-C) with a distance of 21 Å away from the interface at 100 K. No matter whether the PKA is a Cu or C atom, the defect evolution in the Cu bulk follows the trend that the number of defects rises furiously in 0.6 ps and then goes down slowly because of recombination and/or annihilation, finally reaching a stable value after approximately 8 ps (see Fig. 2(a,c)). These profiles are very consistent with those of prior works in metals [26,34, 42]. In particular, the number of interstitials in the Cu bulk is less than that of their vacancies after reaching thermal stability, suggesting that CDIs preferentially trap Cu interstitials over Cu vacancies. Since the phenomenon that C atoms reside in the Cu matrix was not observed in the whole process (discussed in detail below), the surviving defects in the Cu bulk do not contain C components and are all Cu-related defects. On the other hand, the overall trend of defect evolution in the diamond bulk (see Fig. 2(b,d)) exhibits rough consistency with that in the Cu bulk. An interesting phenomenon worth mentioning is that the defect peaks generated by PKA-Cu are higher than those by PKA-C in both the Cu bulk and the diamond bulk.

Nevertheless, several obvious differences in the defect evolutions between diamond bulk and Cu bulk were also found. First, the rising trend of the number of defects in the diamond bulk during the ballistic phase is either tortuous (see Fig. 2(b)) or sharp (see Fig. 2(d)), and the time to defect peak is related to the PKA type (~0.64 ps for PKA-Cu and 0.04 ps for PKA-C). Since no thermal spike was produced in the diamond region [46], the C defect productions in the ballistic phase mainly come from the collision of energetic atoms. In Fig. 2(b), the cascades in diamond were produced by transferring energy from secondary knock-on Cu atoms, while in Fig. 2(d), the lattice displacements of diamond were mainly triggered by a PKA-C. According to the Kinchin−Pease displacement model [35,47], energetic Cu atoms incident into diamond should easily knock out more lattice C atoms, because of their heavy atomic mass and large radius relative to those of C atoms, and then extend the branches of collision sequences in the diamond, eventually causing the difference in ballistic phase between Fig. 2(b,d). Next, the defects in the diamond bulk quickly stabilized (at approximately 1 ps) during the annealing stage, like their response in the ballistic phase. The behaviors are consistent with those observed in other carbon-related materials (e.g., graphite [35], 3C–SiC [48], and pure diamond [46]). The reason may be that the high thermal conductivity of carbon-related materials, relative to that of metals, facilitates heat removal from their cascades [16,49]. Additionally, an opposite phenomenon about the number difference between C interstitials and C vacancies in the diamond bulk occurs in the annealing phase, i.e., the number of C interstitials is either more or less than that of C vacancies, caused by different types of PKAs. In Fig. 2(b), because of the bombardment of energetic Cu atoms with heavy atomic mass, C interstitials will stay away from the displacement region near the CDI, resulting in the separation of vacancy-rich and interstitial-rich regions in the diamond (described in detail below). This behavior has also been observed in the 3C–SiC due to the bombardment of PKA-Si [48]. Consequently, C interstitials were difficult to interact with the CDI because they were far away from the interface, while C vacancies can be affected by the CDI because they were close to the interface, in turn, leaving behind more C interstitials than C vacancies in the diamond bulk. In Fig. 2(d), C interstitials at the end of the collision sequence will surround the vacancy-rich core close to the interface due to the blocking of Cu atoms (described in detail below), so that the CDI may exert influence over both C interstitials and C vacancies. Especially, the characteristic that CDIs preferentially trap interstitials also showed up, and then made the number of C vacancies more than that of C interstitials. Finally, the peak of defects in the Cu bulk is much higher than that in the diamond bulk,
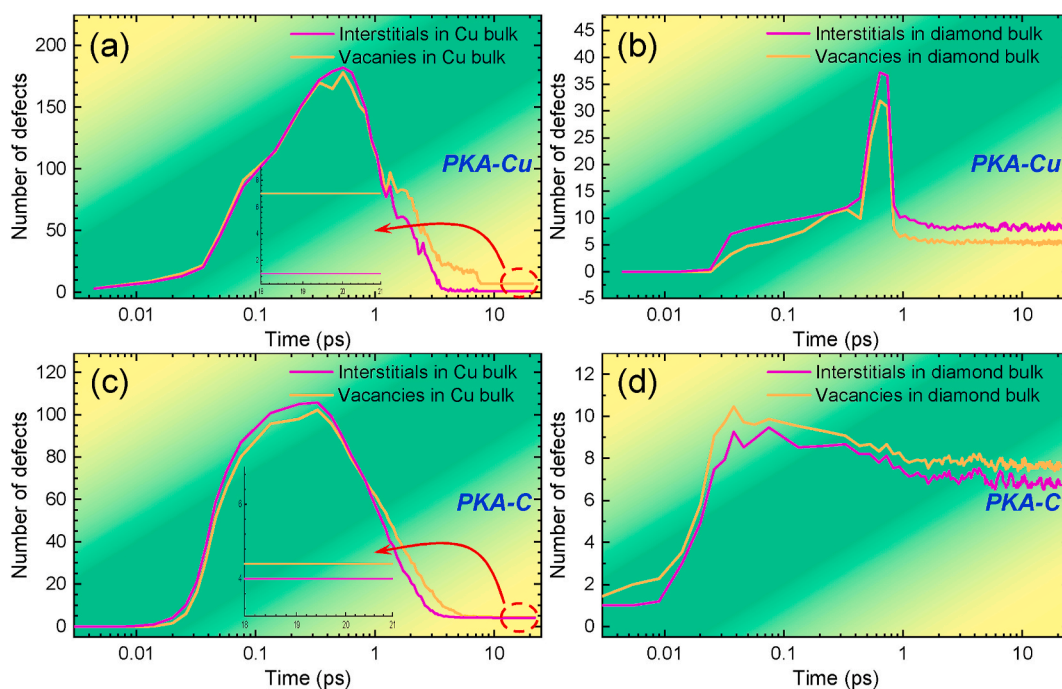

Fig. 2. Time evolution of defect productions initiated by a 5 keV PKA-Cu or PKA-C in CDCs. **(a,b)** Defect productions in Cu bulk (a) and diamond bulk (b) respectively due to a PKA-Cu. **(c,d)** Defect productions in Cu bulk (c) and diamond bulk (d) respectively due to a PKA-C. Note that each curve is a statistical average of 15 runs.

suggesting that displacement cascades are more likely to be produced in the Cu regions of CDCs. This may stem from the effects of thermal spike and the low displacement threshold in Cu relative to diamond [50,51], which also can be indirectly demonstrated by using the SRIM 2013 software package (see Fig. S1) [52].

The atomic configuration of CDCs at displacement spike and its defect distributions at stable phase is exhibited in Fig. 3, for vividly clarifying several phenomena mentioned above. Atomic displacements are recognized by displaying the displacement vectors between atomic positions at 0 and 21 ps in Fig. 3(a,c). The details of the displacement vectors of atoms have been introduced elsewhere [53]. The overall scale of displacement spike initiated by a PKA-Cu is larger than that by a PKA-C, supporting the fact of the defect peak intensities mentioned in Fig. 2. Meanwhile, the profile of displacement cascades produced by a PKA-Cu behaves continuously, while the profile shows sub-cascade branching due to a PKA-C. In both cases, most of the atomic displacements happened in the Cu region, the direct cause of the fourth difference above. Although the degree of atomic displacements in the diamond is low, the C defects produced are very difficult to heal, resulting in a large ratio of n_{C_final}/n_{C_peak} (n_{C_peak} and n_{C_final} represent the numbers of C defects at defect peak and stable phase, respectively) [49]. Near the diamond side of CDI, the sparse and disconnected atom trajectories in Fig. 3(c) that exhibit consistency with those in other carbon-related materials [35,46], make it difficult for the kinetic energy of PKA-C to deposit in a single local region and form a thermal spike, whereas the dense trajectories in Fig. 3(a), approximately like those of metals, may easily lead to higher defect peak in the diamond and prolong the time to defect peak. This can directly clarify the source of the initial differences of defect evolutions between Fig. 2(b,d). Especially,

that many C atom trajectories are away from the interface and point inward the diamond in Fig. 3(a) indicates the gradual separation of C interstitials and C vacancies, while the opposite behavior of trajectories in Fig. 3(c) causes C interstitials and C vacancies not far apart from each other and scattered near the interface. These may result from the differences in collision and energy transfer between Cu and C atoms mentioned above. The behaviors of atomic displacements also ultimately affect the defect distributions of the bulk regions. For example, except for the defects affected by the interface, most of the Cu vacancies are concentrated near the CDI, while the Cu interstitials are mainly distributed in the deep of bulk, as shown in Fig. 3(b,d). At the stable phase, defects mainly remained in the diamond bulk, and the behavior of the interpenetration of Cu and C defects, due to the bombardment of energetic atoms to the interface, did not occur.

3.2. PKA−interface distance effects on irradiation damage

The statistical mean of remnant point defects (*i.e.*, interstitials and vacancies) in the bulk is presented as a function of PKA−interface distance (*d*) in Fig. 4(a). The radial center of CDI is set to be the origin of the axis of *d* in this subsection. The numbers of defects in the Cu bulk and the diamond bulk are counted separately. (**I**) When a PKA-Cu is incident toward the CDI, the number of defects is susceptible to the *d* and tends to increase in the Cu bulk but decrease in the diamond bulk with the increase of *d*. Especially, several numerical curves have prominent intersections around 21 Å, implying that the number of defects in the two different regions of bulk is the closest. Meanwhile, the total number of defects reaches a minimum near the *d* of 21 Å when *d* > 0 Å. When *d* < 21 Å, there are more defects in the diamond bulk, while the number of
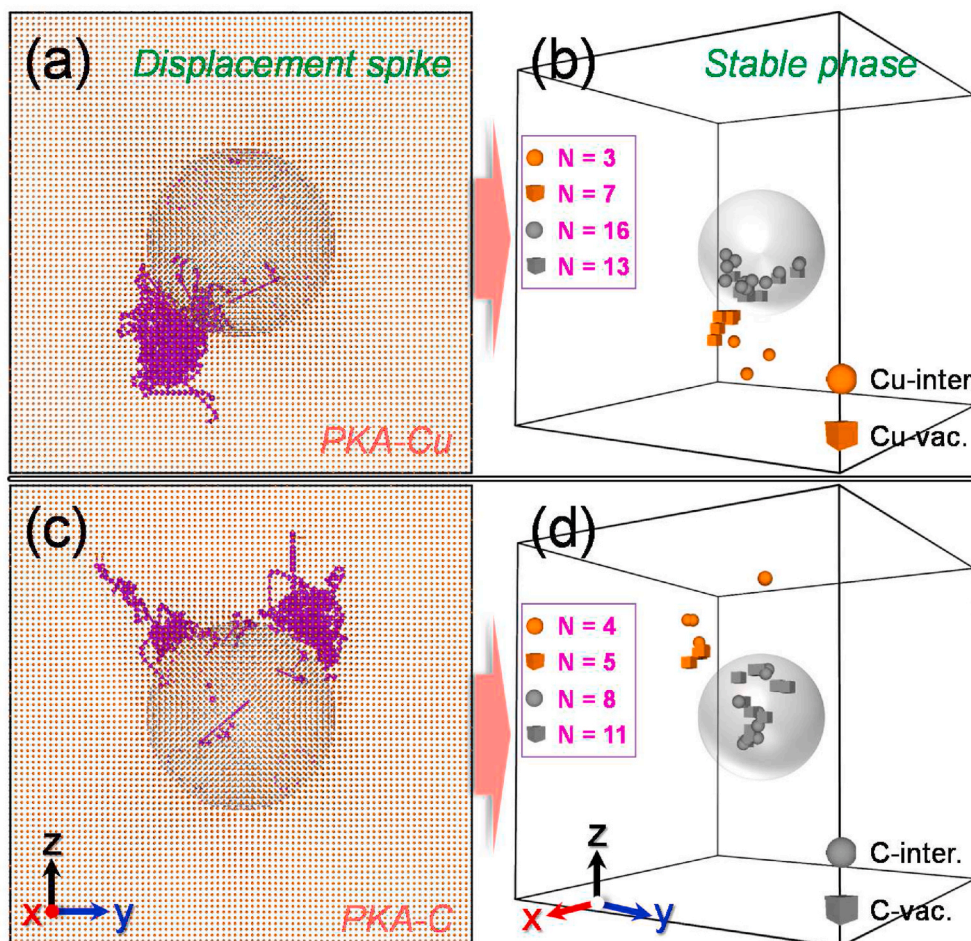

Fig. 3. Atomic displacement configuration within cascade region and its remnant defect distribution in CDCs, produced by a 5 keV PKA-Cu or PKA-C. **(a,b)** Displacement configuration (a) and remnant defects (b) due to a PKA-Cu. **(c,d)** Displacement configuration (c) and remnant defects (d) due to a PKA-C. The purple arrows in the panels (a,c) represent atomic displacement vectors. The number of remnant defects is given in the panels (b,d) according to their types. (For interpretation of the references to colour in this figure legend, the reader is referred to the Web version of this article.)
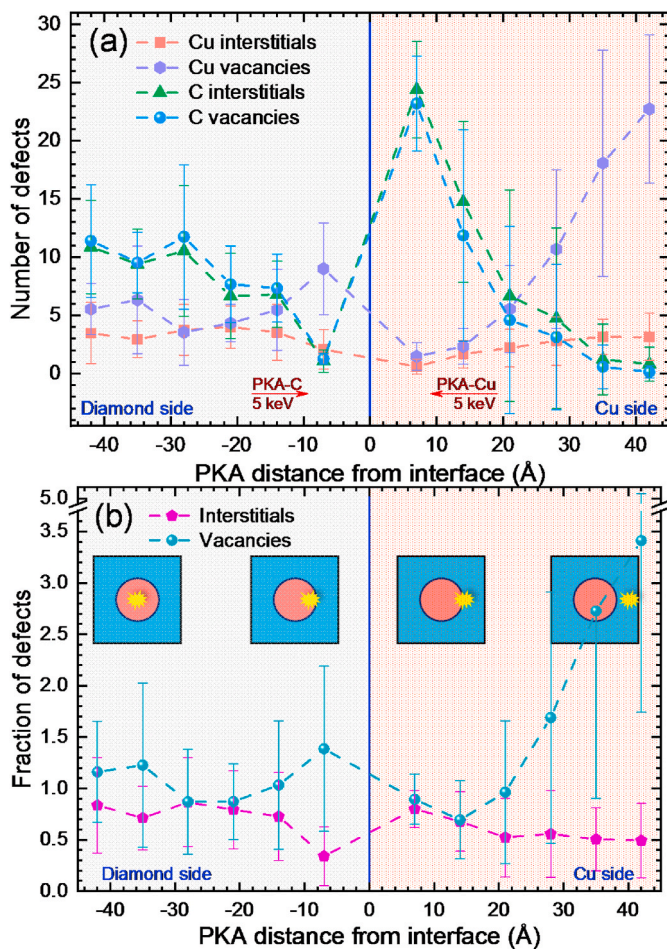
Fig. 4. Statistics of remnant defects produced by a 5-keV PKA at different distances away from the interface at 100 K. **(a)** Number of defects in the bulk as a function of PKA−interface distance. **(b)** Statistically averaged fraction of defects in the bulk as a function of PKA−interface distance. The left and right sides represent diamond and Cu regions, respectively. The cascade region related to certain distance is marked in the inset of panel (b).

defects in the Cu bulk dominates when $d > 21$ Å. The cause can be clarified as follows. The subject of cascade collisions gradually shifts from the diamond region to the Cu region with the increasing d, causing the change of the principal constituent of radiation damage accordingly. Due to the apparent difference of cascade collision processes between the diamond bulk and the Cu bulk when $d > 0$ Å, it is relatively reasonable to use an equivalent cascade parameter $\boldsymbol{p(d)}$ to roughly determine the principal constituent of surviving defects as a function of d (see more details in Appendix A). When $d < 21$ Å, the core of equivalent cascades is in the diamond side and gradually far away from the Cu bulk as the d is reduced, leaving behind high-proportioned C defect productions to regulate $\boldsymbol{p(d)}$. When $d > 21$ Å, the opposite phenomenon occurs, and $\boldsymbol{p(d)}$ is dominated by high-proportioned Cu defects. Around 21 Å, the core of equivalent cascades overlaps with the interface, and the CDI can exert maximum influence on the defect productions, which makes the surviving defect in this situation the least. Furthermore, the number of Cu vacancies is more than that of Cu interstitials when $d > 0$ Å, and the difference between the two gradually increases as the d increases, suggesting that the interface preferentially absorbs Cu interstitials over Cu vacancies. However, the C defects exhibit the opposite behavior again when $d > 0$ Å, the reason for which may stem from the separation of vacancy-rich and interstitial-rich regions in the diamond, as mentioned above. (**II**) When a PKA-C is incident toward the CDI, the number of defects approximately tends to decrease in the diamond bulk

with the increase of d, since more and more C defects are enriched near the interface and thus trapped by the interface as mentioned above. In contrast, almost no specific relationship between the number of Cu defects and the d is presented due to sub-cascade branching in this situation. Whether in the diamond bulk or the Cu bulk, the number of interstitials is less than that of vacancies when $d < 0$ Å, indicating that the characteristic that CDIs preferentially trap interstitials works on both C and Cu elements. (**III**) Over the entire range of d, the number of Cu interstitials fluctuates very little. It has the minimum among all defects in most cases, which may be due to both the high sink efficiency of CDIs for Cu interstitials and the high mobility of Cu interstitials ($\sim$0.1 eV migration energy for Cu interstitial [54], $\sim$0.7 eV for Cu vacancy [54], $\sim$1.6 eV for C interstitial [55], and $\sim$2.3 eV for C vacancy [55]). The difference in the number between C interstitials and C vacancies is little at each d, showing that the biased absorption of C interstitials at the interface is relatively weak, and C interstitials do not load significantly into the interface during cascades. The displacement damage initiated by a PKA-Cu is more significant than that by a PKA-C, because of more energy deposition.

To highlight the impact of CDIs on indiscriminate damage, Fig. 4(b) further exhibits the statistically averaged fraction of defects in the bulk as a function of d. The fraction of defects is defined as

$$F_{defects} = \frac{n_{Cu}^{bulk}}{n_{Cu}} + \frac{n_{diamond}^{bulk}}{n_{diamond}}, \tag{1}$$

where n_X^{bulk} and n_X are the irradiation-induced defect numbers in the Cu (or diamond) bulk and the corresponding single crystal, respectively [56]. Overall, the fraction of vacancies in the bulk is higher than that of interstitials due to the biased absorption at the CDI [54]. The fraction of interstitials is less than 1 over the entire range of d, implying that most of the interstitials surviving upon subsequent annealing after cascade collisions are captured into the CDI because of both the high mobility of interstitials and the thermodynamic driving force of the interface acting on the defects [27,54]. On the other hand, the concentration of vacancies produced in the bulk is close to or higher than that in the single crystals. Especially, the concentration of surviving vacancies produced by a PKA-Cu at $d = 42$ Å is approximately 3.5 times that in the single crystals. These profiles are in good agreement with the behaviors observed in nanocrystalline Cu [54] and Cu–Nb nanolaminates [56]. Consequently, interstitials are preferentially localized at the CDI while vacancies remain immobile in the bulk on a ps time scale of displacement cascades.

3.3. PKA energy effects on irradiation damage

Given the more significant irradiation damage produced by a PKA-Cu relative to a PKA-C in the CDCs, the focus below will be only on the effects of PKA-Cu. Fig. 5(a) shows the surviving defect productions as a function of PKA-Cu energy (E). With the increasing E, the number of surviving defect productions almost linearly increases either in CDCs or in pure Cu (or pure diamond), approximately obeyed the Norgett–Robinson–Torrens (NRT) model [57]. These results are also consistent with those of previous studies [26,42,57]. Notably, the number of Cu defects shows a relatively slight decline at 10 keV compared to that of the normally increasing trend of the NRT model. At each E, the number of interstitials in the Cu bulk is less than that of vacancies, while an opposite behavior occurs in the diamond bulk. This phenomenon is in accordance with that caused by a PKA-Cu at different d and can be explained by the above-mentioned reasons. The degree of irradiation damage is lower in the Cu bulk than that in the diamond bulk at each E because of the relatively high mobility of Cu defects (promoting defect recovery directly demonstrated by the much fewer defects in pure Cu than those in pure diamond) and their efficient absorption by the CDIs. The statistically averaged fraction of defects in the bulk, calculated by using Eq. (1), is further exhibited in Fig. 5(b) as a function
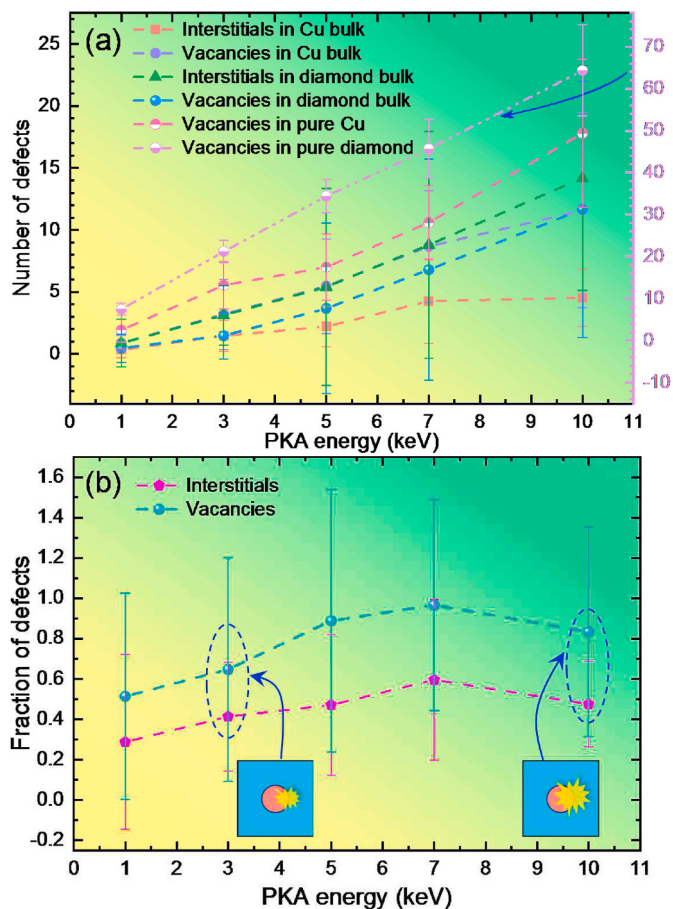
Fig. 5. Statistics of remnant defects produced by a PKA-Cu with different energies near the interface at 100 K. **(a)** Number of defects in the bulk as a function of PKA-Cu energy. **(b)** Statistically averaged fraction of defects in the bulk as a function of PKA-Cu energy. The cascade region related to certain energy is marked in the inset of panel (b).

of E. The fractions of both interstitials and vacancies are not more than 1 at different energies, and the fraction of interstitials is smaller, suggesting that the presence of CDIs helps to promote the self-healing of irradiated defects in the composites relative to the pure counterpart. The fraction of defects reaches its maximum at 7 keV. When $E \leq 7$ keV, the fraction trend keeps consistent with that of the numbers of all defects, while it may be mainly regulated by the Cu defect productions when $E > 7$ keV.

The corresponding configurations of damaged CDCs at displacement spike or stable phase for different E are displayed in Fig. 6(a–e). Through observing the image contrast regulated by atomic density due to cascade collisions, the region of displacement damage can be easily distinguished. With the increase of E, the scale of atom displacements in the CDCs is intensified at displacement spike. At this moment, the disorder in the diamond region keeps the same pace as that in the whole system as the E changes, while the displacements in the Cu region are the most drastic at 7 keV. The reduced displacement spike in the Cu region at 10 keV relative to 7 keV can be explained as follows. The cascades penetrate and cover the diamond region, which dramatically deposits collision energy due to the high displacement threshold in diamond, and in turn reduces the attack on the Cu region. On the other hand, the intense scattering of C atoms causes the secondary transfer of collision energy into the Cu region to come from all directions, which enriches the displaced Cu atoms mainly around the interface rather than deep into the Cu bulk. In this way, the CDI exhibits higher sink efficiency for Cu defects at 10 keV compared to that at other E herein. These explanations may also apply to the abnormal decline of Cu defects at 10 keV in Fig. 5.

At the stable phase for all E, there are almost no apparent signs of atom displacements left in the Cu region. Although the lattice disorder in the diamond region has been recovered to some extent after annealing, the damage profile remains essentially the same as that at displacement spike. To further compare the atomic structural differences, the radial distribution function (RDF), which can provide information about the short-range and long-range crystalline orders of materials, has been adopted and calculated for the undamaged and damaged CDCs according to the following equation [58],

$$g(r) = \frac{V dn(r)}{4\pi r^2 N dr}, \tag{2}$$

where $dn(r)$ represents the number of atoms in the spherical shell from r to $(r + dr)$ for a spherical space of volume V containing N atoms. Fig. 6(f and g) show the RDFs of the CDCs at displacement spike or stable phase as a function of pair separation distance for different E. The RDF of undamaged CDCs is also exhibited in each panel, and thus the differential function between the RDFs of the damaged and undamaged CDCs can be easily obtained. Each peak position of RDF of the CDCs was identified by comparison with those of pure Cu and pure diamond (see Fig. S2). Generally, the RDF of a single crystal has a higher peak at short distances, *e.g.*, 2.575 Å for Cu and 1.525 Å and 2.525 Å for diamond, as observed from Fig. S2. The RDF peak intensities of composites are more significantly influenced by their matrices, resulting in many weak peaks in the positions of the reinforced phase. At displacement spike, the overall RDF peak intensities for each E do not show a sharp change relative to that at 0 ps but only a slight decline. The decline is relatively more pronounced with the increase of E, especially for the peaks at the 1st nearest neighbor (NN) distance of Cu and the 1st and 2nd NN distances of diamond, implying a deterioration of short-range disorder in the CDCs. In addition, the long-range disorder in the diamond region can easily occur (*e.g.*, the disappearance of peaks at 9.525 Å and 9.725 Å) and even be triggered only by a PKA with 1 keV. However, the disorder did not stimulate the transformation of the diamond structure into a graphite structure because of the lack of a distinct peak of sp^2 hybridization of carbon at the distance of 1.420 Å (*i.e.*, the graphite bond length [59]). The value of the differential function is almost always positive at the bottom of each RDF peak. It presents a roughly increasing trend with the increasing E, indicating a gradual broadening of the peak. This reflects the intensified structural disorder originating from the atomic bond elongations that may introduce microstrains [60]. When reaching the stable phase, the disorder has not been effectively eliminated at each E since the differential function is not entirely zeroed. Through comparing the differential functions between Fig. 6(g,f) at each E, it can be found that the short-range disorder of diamond and the long-range disorder of Cu may even be exacerbated after irradiation annealing, such as the peak positions at 1.525 Å for diamond and at 9.225 Å for Cu. All these suggest that irradiation annealing has a limited effect on the damage self-healing of CDCs [26].

3.4. Simulation temperature effects on irradiation damage

The temperature change can make atomic vibration at different degrees, further affecting the atomic model. To avoid inconsistency in the initial crystal structure of bulk due to temperature, the evolution of the CDI model with temperature has been investigated before irradiation and shown in Fig. S3. Indeed, the atomic vibration of CDCs is intensified with the increase of simulation temperature (T). Especially, the atoms within the interface are more apparent in vibration, even triggering a rearrangement of CDI structure above 400 K. However, the T from 100 K to 500 K does not affect the crystal integrity in the bulk. After irradiation annealing, the stable defect production is presented as a function of T in Fig. 7(a). The number of remnant vacancies in pure Cu or pure diamond under the same simulation conditions as those of CDCs is also shown for comparison. As the T elevates, the number of vacancies in pure Cu shows
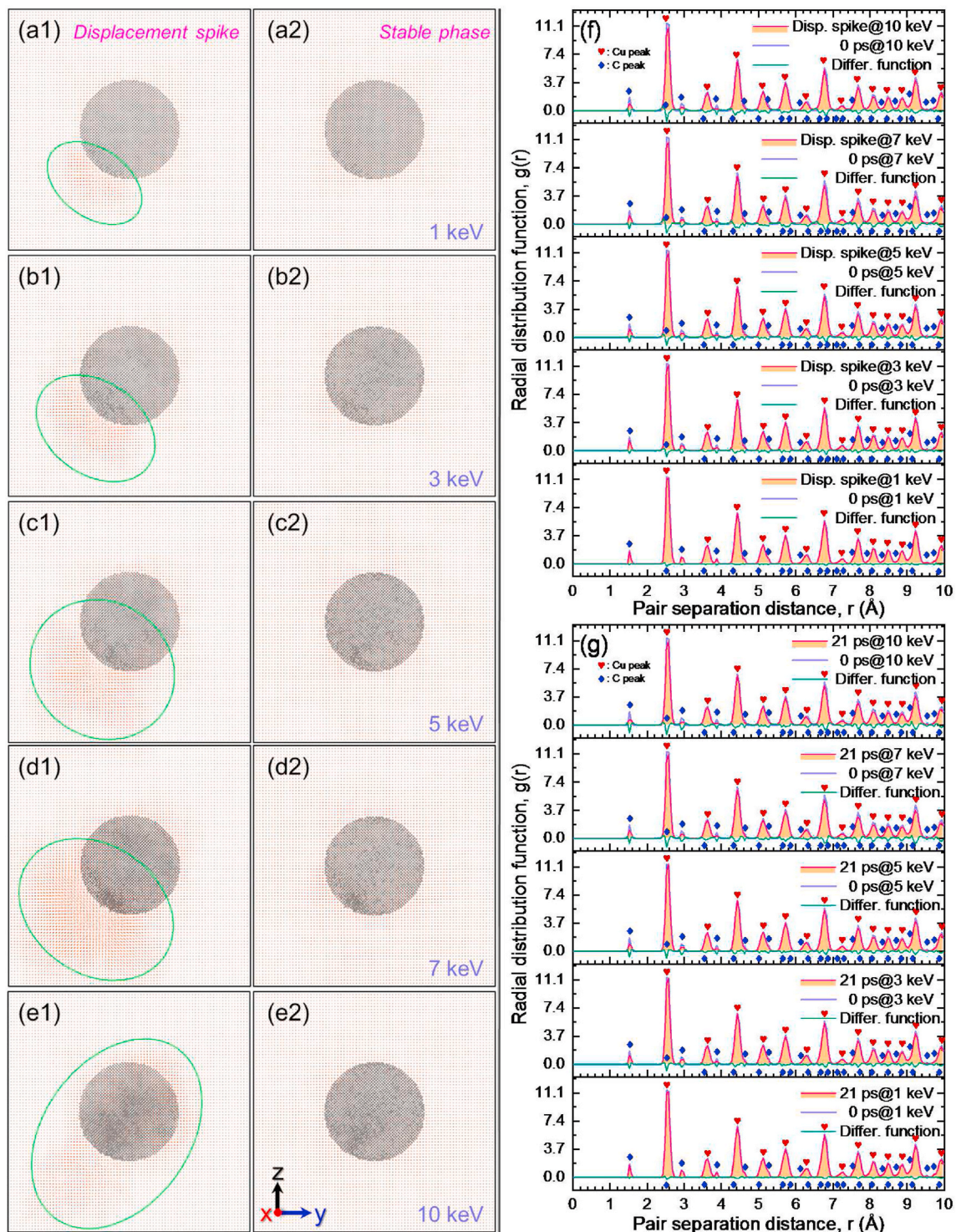
Fig. 6. Damaged configurations of CDCs and corresponding RDFs initiated by a PKA-Cu with varied energies in CDCs at 100 K. **(a–e)** Snapshots of atomic configurations of CDCs at the moments of displacement spike and stable phase caused by a PKA-Cu with 1 (a), 3 (b), 5 (c), 7 (d), or 10 (e) keV. The cascade region is marked by a green oval. **(f,g)** RDFs at the moments of displacement spike (f) and stable phase (g). The RDF of initial CDCs and the differential function are also exhibited in each panel. (For interpretation of the references to colour in this figure legend, the reader is referred to the Web version of this article.)

a declining trend, consistent with the findings in other single crystals [26,57]. This is usually attributed to the accelerated recombination and annihilation of point defects since the essentially immobile vacancies are stimulated to jump by elevated T, like the response of interstitials. In contrast, the trend of defect number in pure diamond with temperature is the opposite, namely, a slight increase, exhibiting consistency with the behavior observed in the 3C–SiC with the same Tersoff potential [48].

Samolyuk et al. [61] suggested that this anomaly may stem from the artificially large migration barriers obtained from the potential. With the increasing T, the number of vacancies in the Cu bulk tends to reduce (like the trend in pure Cu), while the number of Cu interstitials is not sensitive to the T because of their high mobility and efficient absorption by the interface. The number of defects in the diamond bulk first increases, reaches its maximum at approximately 400 K, and thereafter
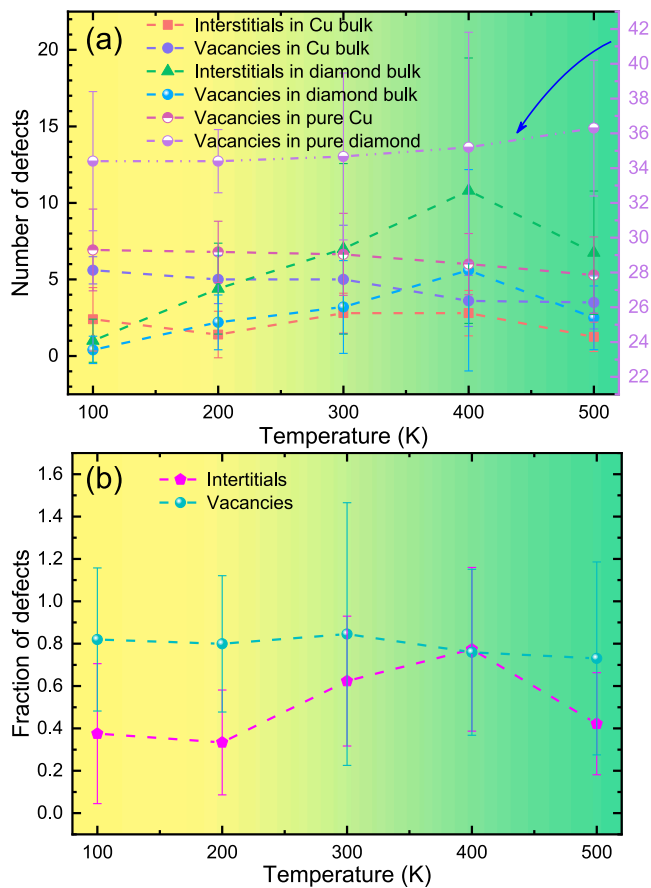
Fig. 7. Statistics of remnant defects produced by a 5-keV PKA-Cu near the interface at different simulation temperatures. **(a)** Number of defects in the bulk as a function of temperature. **(b)** Statistically averaged fraction of defects in the bulk as a function of temperature.

decreases, a trend like that of the graphene damage of Ni–graphene composites in the previous study [26]. Below 400 K, the C defect number of CDCs follows the trend as shown in pure diamond, while the C defects may overcome the barrier to move toward the interface and be trapped by the interface due to activation by the T of above 400 K [56]. On the other hand, the atomic rearrangement that complicates the CDI structure above 400 K may improve the interface energy and further lower the defect formation energy near the interface [62], another reason that reduces the C defects of CDCs. The behavior remains unchanged in the observed temperature range, *i.e.*, the number of interstitials in the Cu bulk is less than that of vacancies while an opposite in the diamond bulk. Around 400 K, the irradiated defects of CDCs are mainly concentrated in the diamond bulk, whereas the degree of displacement damage in the Cu bulk is close to that of the diamond bulk at other temperatures. Based on Eq. (1), the statistically averaged fraction of defects in the bulk is shown in Fig. 7(b) as a function of T. The fraction of defects is less than 1 at each T, once again confirming that CDIs contribute to the self-healing of irradiated defects in the whole system. The fraction of vacancies, due to only the slight fluctuation, is almost independent on the T, originating from the offset by a rise of number for Cu vacancies and a fall of number for C vacancies. The trend that the fraction of interstitials rises and then falls may be mainly regulated by the damage in the diamond bulk. The fraction of interstitials is usually smaller than that of vacancies, but the two tend to be equal at 400 K, implying that the characteristic that CDIs preferentially trap interstitials is independent of T.

Fig. 8(a−e) show the damaged configurations of CDCs at displacement spike or stable phase for each T. During cascade collisions, increasing the temperature will gradually expand the scope of the lattice

disorder, including the regions of Cu and diamond. This comes from the fact that the elevated temperature intensifies atomic vibrations, and atoms are more likely to escape from lattice sites under the shock of cascade collisions. At the stable phase for different T, the atom displacements in the Cu bulk are barely observable, and most of the damage in the diamond bulk is recovered. Especially, the damage rehabilitation rate of diamond bulk is most pronounced at 500 K, consistent with that in Fig. 7. Ulteriorly, the RDFs of the undamaged and damaged CDCs at each T have been calculated and presented in Fig. 8(f and g). The differential function for each case has also been given in the corresponding panel. With the increase of T, the RDF peak intensities of undamaged CDCs gradually reduce, and their half-height peak widths broaden by degrees. Many peaks, particularly at long distances, even disappear after the temperature exceeds 400 K, resulting from the intensification of lattice vibrational frequency triggering the loose lattice arrangement. During irradiation, the RDF peak intensities at displacement spike for each T show slight weakening compared to those at the corresponding initial stage, and the half-height peak widths have tiny broadening. Determining from the differential functions, the weakening and broadening degrees of the peaks are inversely related to temperature, which does not seem to correspond to the enlarged lattice disorder with temperature observed in Fig. 8(a1−e1) since the two results should have a positive correlation in principle [63]. This inconsistency may arise from the strong interference of CDIs on irradiation-induced defects at elevated temperatures, and the cause can be clarified as follows. Despite local lattice disorder due to cascades, the displaced atoms may tend to form the chain-like defects (induced by interfaces) near the CDIs, as like those near α-Fe grain boundaries found by Chen et al. [64]. Instead of those consisting of alternately positioned interstitials and vacancies [64], the chain-like defects at displacement spike are more likely to be in the form of crowdions herein [65] (see Fig. S4) attributing to the synergistic effects of the energetic squeezing of cascades and the interface blocking on displaced atoms [53,66]. This tight defect structure may be beneficial to maintain short-range order, such as still noticeable peak intensities at the distances of 2.575 Å for Cu and 1.525 Å and 2.525 Å for diamond. On the other hand, with the rising of temperature, the influence of CDIs on the formation of chain-like defects is further enhanced because of the intensification of the trapping and/or annihilation capabilities of the interfaces to irradiation defects [56], but almost reaches saturation when $T > 400$ K. Combined with Fig. 7, it can be speculated that the interface capabilities should be largely released when $T > 400$ K. Consequently, the atomic displacement region of CDCs is not hollowed out like that in single crystals [67,68] but forms compact chain-like defects, making it difficult to cause the loosening of lattice structure at elevated temperatures. This may indicate that high ambient temperature has a certain positive effect on inhibiting structural damage of CDCs due to irradiation. At the stable phase, the disorder can be alleviated but not completely removed at each T. Meanwhile, increasing the temperature does not significantly eliminate the residual lattice disorder. Considering that the sink character of CDIs works well and can greatly promote the recombination and/or annihilation of defects in the bulk, the residual disorder may mainly come from the interfacial region, because of the destruction of cascade collisions and the defects captured from the bulk.

4. Conclusions

In the present study, the energetic displacement cascades in CDCs are investigated from the perspectives of PKA−interface distance, PKA energy, and simulation temperature based on atomistic simulations. A summary of the most critical results drawn from this work is as follows:

(a) The defect evolutions have noticeable differences between diamond bulk and Cu bulk in CDCs, mainly manifested in the time to defect peak, the defect annealing rate, the relative ratio of interstitials to vacancies, and the peak intensity of defects. These
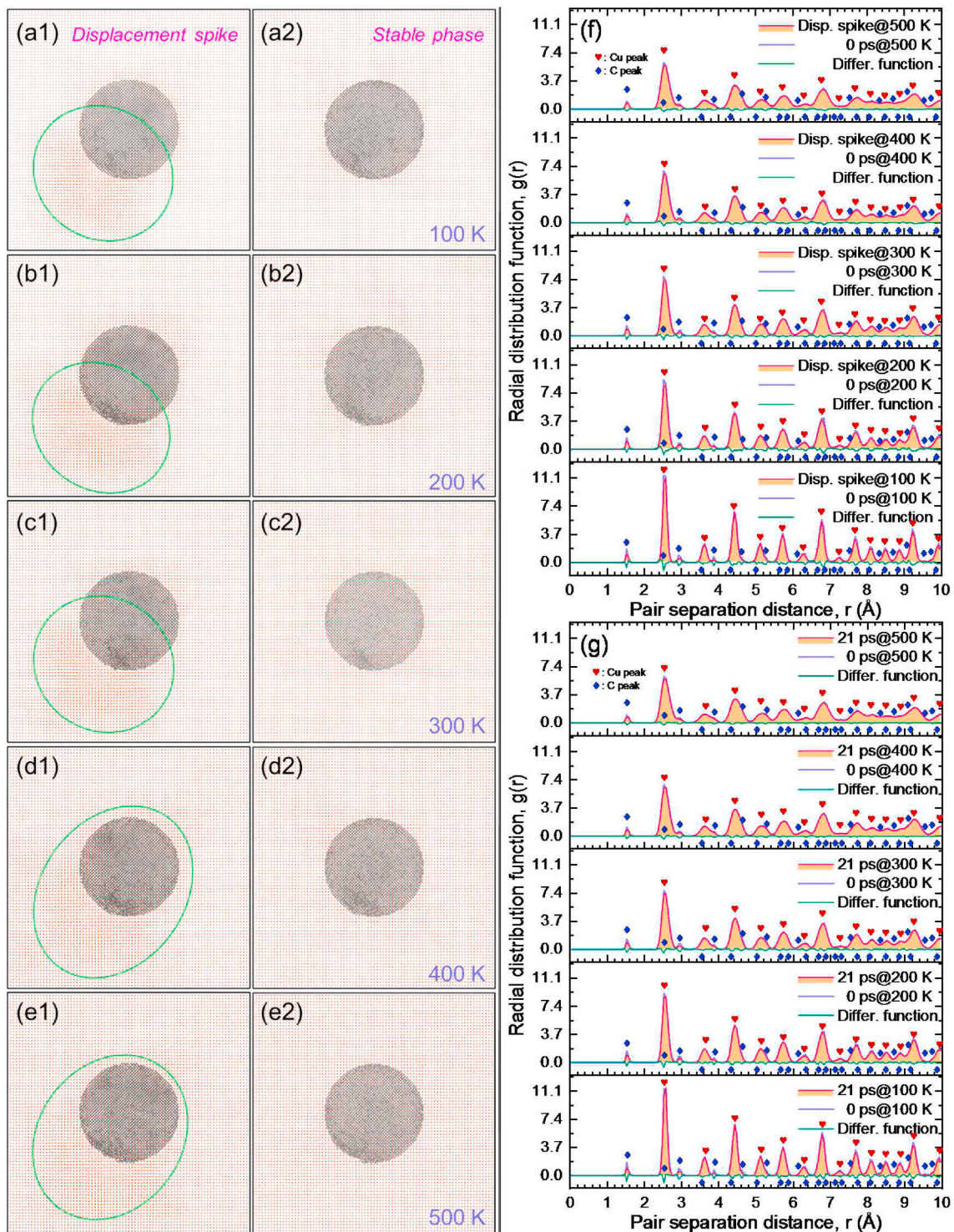
Fig. 8. Damaged configurations of CDCs and corresponding RDFs initiated by a 5-keV PKA-Cu in CDCs at different simulation temperatures. **(a–e)** Snapshots of atomic configurations of CDCs at the moments of displacement spike and stable phase at 100, 200, 300, 400, or 500 K. The cascade region is marked by a green oval. **(f,g)** RDFs at the moments of displacement spike (f) and stable phase (g). The RDF of initial CDCs and the differential function are also exhibited in each panel. (For interpretation of the references to colour in this figure legend, the reader is referred to the Web version of this article.)

can be attributed to the lack of a thermal spike in diamond, the high thermal conductivity of diamond, the differences of collision and energy transfer between Cu and C atoms, and the low displacement threshold in Cu relative to in diamond.

(b) Over the range of d from -42 Å to 42 Å, the statistically averaged fraction of interstitials surviving in the bulk, produced by a PKA with 5 keV at 100 K, is not only lower than that of vacancies but

also no more than 1. Cu interstitials have the lowest concentration among all defects in most cases because of both the high sink efficiency of CDIs for Cu interstitials and the high mobility of Cu interstitials. When the core of equivalent cascades overlaps with the interface (around the d of approximately 21 Å), the total number of defects reaches a minimum for $d > 0$ Å due to the improvement of sink efficiency of CDIs. The displacement

damage initiated by a PKA-Cu is more significant than that by a PKA-C, because of more energy deposition.

(c) With the increase of PKA-Cu energy from 1 keV to 10 keV, the displacement damage in CDCs tends to aggravate. Nevertheless, the fraction of surviving defects always does not exceed 1, and the fraction of interstitials is smaller. A relative decline of damage at 10 keV may result from the dual effects of the cascade penetration through diamond greatly depositing energy and the increasing sink efficiency for Cu defects, which may help for the selection of diamond size in designing CDCs in an irradiated environment. The structural damage is reflected in the short-range disorder of diamond and the long-range disorder of Cu after irradiation, but the transformation of diamond structure into graphite structure has not been observed.

(d) As the *T* elevates from 100 K to 500 K, the number of surviving defects changes in the opposite trend between diamond bulk and Cu bulk in CDCs. However, the fraction of defects is usually less than 1 at each *T*. The capacity of CDIs in trapping defects can be enhanced above 400 K due to the atomic rearrangement of CDI structure and a decline of the defect diffusion barrier. Peculiarly, the atomic displacement region of CDCs may form compact chain-like defects to inhibit the loosening of lattice structures at elevated temperatures. In addition, increasing the temperature does not significantly eliminate the residual lattice disorder.

Overall, CDIs have a positive help in promoting the recombination and/or annihilation of irradiation defects from Cu bulk and diamond bulk throughout the process and preferentially absorbing interstitials over vacancies, which improves the ability of CDCs in healing irradiation defects. The current investigation significantly facilitates our understanding of the irradiation effects in CDCs. It can provide a reference for assessing the irradiation tolerance of the composites acting as thermal management materials for spacecraft electronics.

Declaration of competing interest

The authors declare that they have no known competing financial interests or personal relationships that could have appeared to influence the work reported in this paper.

Acknowledgments

Appendix B. Supplementary data

Supplementary data to this article can be found online at https://doi.org/10.1016/j.ceramint.2022.02.232.

Appendix A. Description of equivalent cascade parameter of CDCs

Given the distinct difference between Cu and diamond in displacement cascades, adopting an equivalent cascade model to evaluate the effect of a CDI on the irradiation damage evolutions of the two in the same situation is relatively doable, especially for the case of PKA-Cu inducing cascades without sub-cascade branching. The equivalent cascades in CDCs can use a parameter $p(d)$ (a function with mirror symmetry about a certain d) to roughly describe based on our statistical analysis herein. The $p(d)$ represents the residual rate of displaced defects within equivalent cascades produced by a PKA at a certain distance away from the interface, and its estimated formula can be written as

$$p(d) \propto \frac{n_{C\_final}(d)}{n_{C\_peak}(d)} + \frac{n_{Cu\_final}(d)}{n_{Cu\_peak}(d)}, \tag{A.1}$$

where $n_{X\_peak}(d)$ and $n_{X\_final}(d)$ denote the numbers of X (*i.e.*, C or Cu) defects in the bulk at defect peak and stable phase, respectively. When a PKA is infinitely far away from the interface, the value of $p(d)$ will tend to be equal to $\frac{n_{C\_final}(d)}{n_{C\_peak}(d)}$ or $\frac{n_{Cu\_final}(d)}{n_{Cu\_peak}(d)}$, while the value of $p(d)$ has a minimum when the core of equivalent cascades overlaps with the interface. For example, through observing Figs. 2 and 3, it is easy to distinguish the difference of defect evolutions produced by a 5-keV PKA-Cu between the Cu bulk and the diamond bulk, *i.e.*, higher displacement spike but fewer surviving defects in the Cu bulk relative to those in the diamond bulk. By extracting the values of peak defects and stable defects from Figs. 2 and 3, and then substituting them into Eq. (A.1), the profile of $p(d)$ versus PKA−interface distance at 100 K can be obtained and shown in Fig. (A1). The $p(d)$ is almost symmetric about approximately 25 Å.
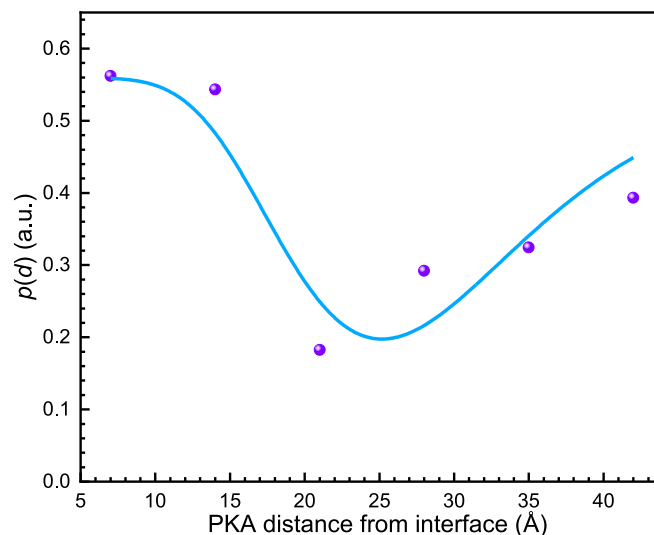
Fig. A1. Equivalent cascade parameter of CDCs as a function of PKA−interface distance, produced by a 5-keV PKA at 100 K.

References

[1] D. Sternberg, J. Essmiller, C. Colley, A. Klesh, J. Krajewski, Attitude control system for the Mars cube one spacecraft, IEEE Aerosp. Conf. (2019) 1–10, https://doi.org/10.1109/AERO.2019.8741816.

[2] O. Kodheli, E. Lagunas, N. Maturo, S.K. Sharma, B. Shankar, J.F.M. Montoya, J.C. M. Duncan, D. Spano, S. Chatzinotas, S. Kisseleff, J. Querol, L. Lei, T.X. Vu, G. Goussetis, Satellite communications in the new space era: a survey and future challenges, IEEE Commun. Surv. Tutor. 23 (2020) 70–109, https://doi.org/10.1109/COMST.2020.3028247.

[3] F. Aguirre, D. Schatzel, High density packaging technologies for RF electronics in small spacecraft, IEEE Aerosp. Conf (2017) 1–11, https://doi.org/10.1109/AERO.2017.7943745.

[4] M.T. Barako, V. Gambin, J. Tice, Integrated nanomaterials for extreme thermal management: a perspective for aerospace applications, Nanotechnology 15 (2018) 154003, https://doi.org/10.1088/1361-6528/aaabe1.

[5] L. Lei, L. Bolzoni, F. Yang, High thermal conductivity and strong interface bonding of a hot-forged Cu/Ti-coated-diamond composite, Carbon 168 (2020) 553–563, https://doi.org/10.1016/j.carbon.2020.07.001.

[6] C. Zweben, Ultrahigh-thermal-conductivity packaging materials, 21st IEEE SEMI-THERM Symp. Proc., (2005): 168–174, https://doi.org/10.1109/STHERM.2005.1412174.

[7] Z.C. Du, M.R. Zhu, Z.G. Wang, J.G. Yang, Design and application of composite platform with extreme low thermal deformation for satellite, Compos. Struct. 152 (2016) 693–703, https://doi.org/10.1016/j.compstruct.2016.05.073.

[8] Z.C. Du, H.F. Hou, Z.G. Wang, J.G. Yang, Thermal deformation isolation for satellite platforms via flexible connections, Int. J. Precis. Eng. Manuf. 18 (2017) 1821–1832, https://doi.org/10.1007/s12541-017-0211-4.

[9] J. Barcena, J. Maudes, M. Vellvehi, X. Jorda, I. Obieta, C. Guraya, L. Bilbao, C. Jiménez, C. Merveille, J. Coleto, Innovative packaging solution for power and thermal management of wide-bandgap semiconductor devices in space applications, Acta Astronaut. 62 (2008) 422–430, https://doi.org/10.1016/j.actaastro.2008.01.010.

[10] A.L. Moore, L. Shi, Emerging challenges and materials for thermal management of electronics, Mater. Today 17 (2014) 163–174, https://doi.org/10.1016/j.mattod.2014.04.003.

[11] X.H. Qu, L. Zhang, M. Wu, S.B. Ren, Review of metal matrix composites with high thermal conductivity for thermal management applications, Prog. Nat. Sci. 21 (2011) 189–197, https://doi.org/10.1016/S1002-0071(12)60029-X.

[12] C. Zhou, D. Chen, X.B. Zhang, Z. Chen, S.Y. Zhong, Y. Wu, G. Ji, H.W. Wang, The roles of geometry and topology structures of graphite fillers on thermal conductivity of the graphite/aluminum composites, Phys. Lett. A 397 (2015) 452–457, https://doi.org/10.1016/j.physleta.2014.10.048.

[13] C.L. Wei, J.G. Cheng, M. Zhang, R. Zhou, B.Z. Wei, X.X. Yu, L.M. Luo, P.Q. Chen, Fabrication of diamond/W–Cu functionally graded material by microwave sintering, Nucl. Eng. Technol. (2021), https://doi.org/10.1016/j.net.2021.08.035 (In Press).

[14] S.V. Kidalov, F.M. Shakhov, Thermal conductivity of diamond composites, Materials 2 (2009) 2467–2495, https://doi.org/10.3390/ma2042467.

[15] S.G. Dai, J.W. Li, N.X. Lu, Research progress of diamond/copper composites with high thermal conductivity, Diam. Relat. Mater. 108 (2020) 107993, https://doi.org/10.1016/j.diamond.2020.107993.

[16] B. Xu, S.W. Hung, S.Q. Hu, C. Shao, R.L. Guo, J. Choi, T. Kodama, F.R. Chen, J. Shiomi, Scalable monolayer-functionalized nanointerface for thermal

conductivity enhancement in copper/diamond composite, Carbon 175 (2021) 299–306, https://doi.org/10.1016/j.carbon.2021.01.018.

[17] S.Q. Jia, L. Bolzoni, T. Li, F. Yang, Unveiling the interface characteristics and their influence on the heat transfer behavior of hot-forged Cu–Cr/diamond composites, Carbon 172 (2021) 390–401, https://doi.org/10.1016/j.carbon.2020.10.036.

[18] E.G. Stassinopoulos, J.P. Raymond, The space radiation environment for electronics,, P. IEEE 76 (1988) 1423–1442, https://doi.org/10.1109/5.90113.

[19] J.W. Wilson, J.L. Shinn, R.K. Tripathi, R.C. Singleterry, M.S. Clowdsley, S. A. Thibeault, F.M. Cheatwood, W. Schimmerling, F.A. Cucinotta, G.D. Badhwar, A. K. Noor, M.Y. Kim, F.F. Badavi, J.H. Heinbockel, J. Miller, C. Zeitlin, L. Heilbronn, Issues in deep space radiation protection, Acta Astronaut. 49 (2001) 289–312, https://doi.org/10.1016/S0094-5765(01)00107-2.

[20] J.A. Wang, R.C. Singleterry Jr., R.J. Ellis, H.T. Hunter, Radiation effects on spacecraft structural materials, Proc. Int. Conf. Adv. Nucl. Power Plants 40 (2002) 1–9.

[21] A.K. Geremew, F. Kargar, E.X. Zhang, S.E. Zhao, E. Aytan, M.A. Bloodgood, T. T. Salguero, S. Rumyantsev, A. Fedoseev, D.M. Fleetwood, A.A. Balandin, Proton-irradiation-immune electronics implemented with two-dimensional charge-density-wave devices, Nanoscale 11 (2019) 8380–8386, https://doi.org/10.1039/c9nr01614g.

[22] N. Kato, M. Sugiyam, Electron irradiation resistance of NiO/ZnO visible-light-transparent solar cells, Jpn. J. Appl. Phys. 59 (2020) 101004, https://doi.org/10.35848/1347-4065/abb983.

[23] Z.N. Xie, H. Guo, X.M. Zhang, Influence of Space Environment on the properties of diamond/Cu composites, Chin. Mater. Conf. (2018) 117–122, https://doi.org/10.1007/978-981-13-5944-6_12.

[24] X.H. Zhang, K. Hattar, Y.X. Chen, L. Shao, J. Li, C. Sun, K.Y. Yu, N. Li, M.L. Taheri, H.Y. Wang, J. Wang, M. Nastasi, Radiation damage in nanostructured materials, Prog. Mater. Sci. 96 (2018) 217–321, https://doi.org/10.1016/j.pmatsci.2018.03.002.

[25] J. Chen, K. Dang, H.T. Vo, P. Hosemann, S.J. Fensin, Associating GB characteristics with its sink efficiency in absorbing Frank loops in Cu, Scripta Mater. 192 (2021) 61–66, https://doi.org/10.1016/j.scriptamat.2020.10.006.

[26] H. Huang, B. Cai, H. Li, X.T. Yuan, Y.N. Jin, Atomistic simulation of energetic displacement cascades near an Ni–graphene interface, J. Supercrit. Fluids 170 (2021) 105162, https://doi.org/10.1016/j.supflu.2021.105162.

[27] H. Huang, X.B. Tang, K. Xie, Q. Peng, Enhanced self-healing of irradiation defects near a Ni–graphene interface by damaged graphene: insights from atomistic modeling, J. Phys. Chem. Solid. 151 (2021) 109909, https://doi.org/10.1016/j.jpcs.2020.109909.

[28] H.F. Huang, W. Zhang, M. De Los Reyes, X.L. Zhou, C. Yang, R. Xie, X.T. Zhou, P. Huai, H.J. Xu, Mitigation of He embrittlement and swelling in nickel by dispersed SiC nanoparticles, Mater. Des. 90 (2016) 359–363, https://doi.org/10.1016/j.matdes.2015.10.147.

[29] K.P. So, D. Chen, A. Kushima, M. Li, S. Kim, Y. Yang, Z. Wang, J.G. Park, Y.H. Lee, R.I. Gonzalez, M. Kiwi, E.M. Bringa, L. Shao, J. Li, Dispersion of carbon nanotubes in aluminum improves radiation resistance, Nano Energy 22 (2016) 319–327, https://doi.org/10.1016/j.nanoen.2016.01.019.

[30] J. Tang, G. Wei, X.C. Cai, S.L. Hu, T.D. Shen, T. Cheng, R. Yin, J. Zhang, X.F. Ruan, B. Yang, Y.Q. Wang, G.X. Cai, C.Z. Jiang, F. Ren, Smart 3D network nanocomposites collect irradiation-induced "trash", Matter 3 (2020) 1631–1645, https://doi.org/10.1016/j.matt.2020.08.010.

[31] K.M. Yang, P.Z. Tang, Q. Zhang, H.Y. Ma, E.Q. Liu, M. Li, X. Zhang, J. Li, Y. Liu, T. X. Fan, Enhanced defect annihilation capability of the graphene/copper interface:

an in situ study, Scripta Mater. 203 (2021) 114001, https://doi.org/10.1016/j.scriptamat.2021.114001.

[32] T.L. Yang, L. Yang, H. Liu, H.L. Zhou, S.M. Peng, X.S. Zhou, F. Gao, X.T. Zu, Ab initio study of stability and migration of point defects in copper-graphene layered composite, J. Alloys Compd. 692 (2017) 49–58, https://doi.org/10.1016/j.jallcom.2016.08.311.

[33] K. Nordlund, F. Djurabekova, Multiscale modelling of irradiation in nanostructures, J. Comput. Electron. 13 (2014) 122–141, https://doi.org/10.1007/s10825-013-0542-z.

[34] R. Collette, J. King, Molecular dynamics simulations of radiation cascade evolution near cellular dislocation structures in additively manufactured stainless steels, J. Nucl. Mater. 549 (2021) 152872, https://doi.org/10.1016/j.jnucmat.2021.152872.

[35] H.J. Christie, M. Robinson, D.L. Roach, D.K. Ross, Simulating radiation damage cascades in graphite, Carbon 81 (2015) 105–114, https://doi.org/10.1016/j.carbon.2014.09.031.

[36] S. Plimpton, Fast parallel algorithms for short-range molecular dynamics, J. Comput. Phys. 117 (1995) 1–19, https://doi.org/10.1006/jcph.1995.1039.

[37] A. Stukowski, Visualization and analysis of atomistic simulation data with OVITO–the Open Visualization Tool, Model. Simulat. Mater. Sci. Eng. 18 (2009), https://doi.org/10.1088/0965-0393/18/1/015012, 015012.

[38] M.J. Demkowicz, R.G. Hoagland, Simulations of collision cascades in Cu–Nb layered composites using an EAM interatomic potential, Int. J. Appl. Mech. 1 (2009) 421–442, https://doi.org/10.1142/S1758825109000216.

[39] R. Devanathan, T. Diaz de la Rubia, W.J. Weber, Displacement threshold energies in β-SiC, J. Nucl. Mater. 253 (1998) 47–52, https://doi.org/10.1016/S0022-3115(97)00304-8.

[40] S.P. Huang, D.S. Mainardi, P.B. Balbuena, Structure and dynamics of graphite-supported bimetallic nanoclusters, Surf. Sci. 545 (2003) 163–179, https://doi.org/10.1016/j.susc.2003.08.050.

[41] J.F. Ziegler, J. Biersack, U. Littmark, The Stopping and Range of Ions in Matter, vol. 1, Pergamon, New York, 1985.

[42] F.D. Chen, X.B. Tang, Y.H. Yang, H. Huang, J. Liu, H. Li, D. Chen, Atomic simulations of Fe/Ni multilayer nanocomposites on the radiation damage resistance, J. Nucl. Mater. 468 (2016) 164–170, https://doi.org/10.1016/j.jnucmat.2015.11.028.

[43] J.C. Bourgoin, R. Kiliulis, C. Gonzales, G. Strobl, C. Flores, K. Bogus, C. Signorini, Deep Space Degradation of Si and GaAs Solar Cells, 25th IEEE Photovolt. Specialists Conf., 1996, pp. 211–214, https://doi.org/10.1109/PVSC.1996.563984.

[44] M. Elbuluk, A. Hammoud, R. Patterson, Power Electronic Components, Circuits and Systems for Deep Space Missions, 36th IEEE Power Electron, Specialists Conf., 2005, pp. 1156–1162, https://doi.org/10.1109/PESC.2005.1581775.

[45] W.D. Guo, G.C. Fu, B. Wan, M. Zhu, Reconstruction of pressureless sintered micron silver joints and simulation analysis of elasticity degradation in deep space environment, Appl. Sci. 10 (2020) 6368, https://doi.org/10.3390/app10186368.

[46] J.T. Buchan, M. Robinson, H.J. Christie, D.L. Roach, D.K. Ross, N.A. Marks, Molecular dynamics simulation of radiation damage cascades in diamond, J. Appl. Phys. 117 (2015) 245901, https://doi.org/10.1063/1.4922457.

[47] G.S. Was, Fundamentals of Radiation Materials Science, second ed., Springer-Verlag, Berlin Heidelberg, 2017.

[48] Q. Ran, Y. Zhou, Y. Zou, J. Wang, Z.G. Duan, Z.P. Sun, B.Q. Fu, S.X. Gao, Molecular dynamics simulation of displacement cascades in cubic silicon carbide, Nucl. Mater. Energy 27 (2021) 100957, https://doi.org/10.1016/j.nme.2021.100957.

[49] M.W. Finnis, P. Agnew, A.J.E. Foreman, Thermal excitation of electrons in energetic displacement cascades, Phys. Rev. B 44 (1991) 567, https://doi.org/10.1103/PhysRevB.44.567.

[50] J.C. Bourgoin, B. Massarani, Threshold energy for atomic displacement in diamond, Phys. Rev. B 14 (1976) 3690, https://doi.org/10.1103/PhysRevB.14.3690.

[51] W.G. Wolfer, Fundamental properties of defects in metals, Compre. Nucl. Mater. 1 (2012) 1–45.

[52] J.F. Ziegler, M.D. Ziegler, J.P. Biersack, SRIM–The stopping and range of ions in matter, Nucl. Instrum. Methods B 268 (2010) 1818–1823, https://doi.org/10.1016/j.nimb.2010.02.091, 2010.

[53] H. Huang, X.B. Zhou, F.D. Chen, J. Liu, D. Chen, Role of graphene layers on the radiation resistance of copper–graphene nanocomposite: inhibiting the expansion of thermal spike, J. Nucl. Mater. 493 (2017) 322–329, https://doi.org/10.1016/j.jnucmat.2017.06.023.

[54] X.M. Bai, A.F. Voter, R.G. Hoagland, M. Nastasi, B.P. Uberuaga, Efficient annealing of radiation damage near grain boundaries via interstitial emission, Science 327 (2010) 1631–1634, https://doi.org/10.1126/science.1183723.

[55] J.W. Steeds, Orientation dependence of near-threshold damage production by electron irradiation of 4H SiC and diamond and outward migration of defects, Nucl. Instrum. Methods B 269 (2011) 1702–1706, https://doi.org/10.1016/j.nimb.2010.12.029.

[56] X.Y. Liu, B.P. Uberuaga, M.J. Demkowicz, T.C. Germann, A. Misra, M. Nastasi, Mechanism for recombination of radiation-induced point defects at interphase boundaries, Phys. Rev. B 85 (2012) 012103, https://doi.org/10.1103/PhysRevB.85.012103, 012103.

[57] D.J. Bacon, F. Gao, Y.N. Osetsky, The primary damage state in fcc, bcc and hcp metals as seen in molecular dynamics simulations, J. Nucl. Mater. 276 (2000) 1–12, https://doi.org/10.1016/S0022-3115(99)00165-8.

[58] C.Z. Zhu, X.F. Liu, X.L. Yu, N. Zhao, J.H. Liu, J. Xu, A small-angle X-ray scattering study and molecular dynamics simulation of microvoid evolution during the tensile deformation of carbon fibers, Carbon 50 (2012) 235–243, https://doi.org/10.1016/j.carbon.2011.08.040.

[59] D.W. Boukhvalov, M.I. Katsnelson, A.I. Lichtenstein, Hydrogen on graphene: electronic structure, total energy, structural distortions and magnetism from first-principles calculations, Phys. Rev. B 77 (2008), https://doi.org/10.1103/PhysRevB.77.035427, 035427.

[60] M. Wojdyr, Y. Mo, E. Grzanka, S. Stelmakh, S. Gierlotka, T. Proffen, T.W. Zerda, B. Palosz, I. Szlufarska, Transition of nc-SiC powder surface into grain boundaries during sintering by molecular dynamics simulation and neutron powder diffraction, 10th Eur. Powder Diffr. Conf. (2015) 255–260, https://doi.org/10.1524/9783486992540-040.

[61] G.D. Samolyuk, Y.N. Osetsky, R.E. Stoller, Molecular dynamics modeling of atomic displacement cascades in 3C–SiC: comparison of interatomic potentials, J. Nucl. Mater. 465 (2015) 83–88, https://doi.org/10.1016/j.jnucmat.2015.05.036.

[62] X.M. Bai, L.J. Vernon, R.G. Hoagland, A.F. Voter, M. Nastasi, B.P. Uberuaga, Role of atomic structure on grain boundary-defect interactions in Cu, Phys. Rev. B 85 (2012) 214103, https://doi.org/10.1103/PhysRevB.85.214103.

[63] S. Rawat, P.M. Raole, Molecular dynamics investigation of void evolution dynamics in single crystal iron at extreme strain rates, Comput. Mater. Sci. 154 (2018) 393–404, https://doi.org/10.1016/j.commatsci.2018.08.010.

[64] D. Chen, J. Wang, T.Y. Chen, L. Shao, Defect annihilation at grain boundaries in alpha-Fe, Sci. Rep. 3 (2013) 1–5, https://doi.org/10.1038/srep01450.

[65] D. Chen, L. Shao, Molecular dynamics simulation of ion focusing and crowdion formation in self-ion-irradiated Fe, Nucl. Instrum. Methods B 272 (2012) 33–36, https://doi.org/10.1016/j.nimb.2011.01.027.

[66] C.G. Zhang, Y.G. Li, W.H. Zhou, L. Hu, Z. Zeng, Anti-radiation mechanisms in nanoporous gold studied via molecular dynamics simulations, J. Nucl. Mater. 466 (2015) 328–333, https://doi.org/10.1016/j.jnucmat.2015.08.003.

[67] T. Diaz de la Rubia, R.S. Averback, R. Hsieh, R. Benedek, Molecular dynamics simulation of displacement cascades in Cu and Ni: thermal spike behavior, J. Mater. Res. 4 (1989) 579–586, https://doi.org/10.1557/JMR.1989.0579.

[68] V.I. Protasov, V.G. Chudinov, Evolution of cascade region during the thermal spike, Radiat. Eff. 66 (1982) 1–7, https://doi.org/10.1080/00337578208211468.